Chinese Chemical Letters 32 (2021) 1795–1798

Contents lists available at ScienceDirect

Chinese Chemical Letters

journal homepage: www.elsevier.com/locate/cclet

Communication

Revealing HOCl burst from endoplasmic reticulum in cisplatin-treated cells *via* a ratiometric fluorescent probe

Shan Wang[a,d,1], Beitong Zhu[b,1], Bingya Wang[d], Xinhua Cao[d], Lei Zhu[a], Ji-Ting Hou[c,d,**], Lintao Zeng[a,b,*]

[a] Institute of Biomedical Materials Industry Technology, Hubei Engineering University, Xiaogan 432000, China
[b] College of Light Industry and Food Engineering, Guangxi University, Nanning 530004, China
[c] Key Laboratory of Emergency and Trauma, Ministry of Education, Key Laboratory of Hainan Trauma and Disaster Rescue, College of Emergency and Trauma, Hainan Medical University, Haikou 571199, China
[d] College of Chemistry and Chemical Engineering, Xinyang Normal University, Xinyang 464000, China

ARTICLE INFO

Article history:
Received 27 October 2020
Received in revised form 21 December 2020
Accepted 23 December 2020
Available online 25 December 2020

Keywords:
Fluorescent probes
Ratiometric
HOCl
Endoplasmic reticulum
Cisplatin

ABSTRACT

The reactive oxygen species (ROS) are tightly associated with endoplasmic reticulum (ER) stress. Thus, the deep and visual insight of aberrant ROS fluctuations in the ER can help us better investigate the ER stress-associated pathology. In this work, a fluorescent probe ERC for HOCl detection in the ER based on phenothiazine-derived coumarin platform was developed. In the presence of HOCl, ERC exhibited an emission change from 609 nm to 503 nm within seconds. It also showed high sensitivity (0.44 μmol/L) and superb photostability. Significantly, ERC displayed low cytotoxicity, good cell membrane permeability, and appreciable ER-targetability. Ultimately, the probe was successfully utilized to image exogenous and endogenous HOCl in living cells and reveal the HOCl burst in cisplatin-treated cancer cells.

As the largest organelle in eukaryotes, the endoplasmic reticulum (ER) plays essential roles in in the cellular processes, such as synthesis, folding, modification, and delivery of proteins [1], and the primary storage of intracellular Ca^{2+} [2]. However, the dysfunction of ER, generally termed as ER stress, has been found to induce cell death and even involve various diseases [3–6]. On the other hand, reactive oxygen species (ROS, including $^{\bullet}OH$, $O_2^{\bullet-}$, $ONOO^-$, H_2O_2, ClO^-, and $^1O_2$) crucially work during the protein synthesis and folding through the disulfide bond formation [7]. Therefore, the overexpressed ROS in the ER would cause oxidative stress, leading to unfolded protein response that can cause ER stress [8]. Accordingly, the deep and visual insight of aberrant ROS fluctuations in the ER can help us better investigate the ER stress-associated pathology [9]. However, it is well known that the vast majority of ROS is produced and consumed in mitochondria [10], and much less ROS are generated in the other organelles including the ER. Thus, monitoring ROS variations within the ER remains a big challenge owing to the lack of adequately sensitive detecting techniques and the shortage of ER-targeting methods.

Due to its high sensitivity and superb spatiotemporal resolution, fluorimetric analysis has been applied to trace the events in biosystems in the last decades [7,11–16]. In the past five years, a handful of fluorescent probes have also been developed to detect various ROS in the ER on account of the increasing knowledge of ER-ROS association and the development of ER-targeting techniques [17–27]. Nevertheless, most of the probes gave intensity-based signal response toward ROS changes, which might be influenced by the variations of ER microenvironment or instrumental perturbation [17–21,24,18–27]. By contrast, ratiometric fluorescent probes exhibiting fluorescence changes at dual emission bands can avoid these interference sources with built-in correction [28,29]. Hence, it is highly desirable to devise ratiometric fluorescent probes for ROS detection involved in ER stress for more precise evaluation of certain pathological processes.

In this respect, we described a fluorescent probe ERC for HOCl detection in the ER based on a phenothiazine-derived coumarin platform that has been developed by our group and others [30–33]. The sulfur atom of phenothiazine-derived coumarin can be

* Corresponding author at: Institute of Biomedical Materials Industry Technology, Hubei Engineering University, Xiaogan 432000, China.
** Corresponding author at: Key Laboratory of Emergency and Trauma, Ministry of Education, Key Laboratory of Hainan Trauma and Disaster Rescue, College of Emergency and Trauma, Hainan Medical University, Haikou 571199, China.
E-mail addresses: houjiting2206@163.com (J.-T. Hou), zlt1981@126.com (L. Zeng).
[1] These authors contributed equally to this work.

https://doi.org/10.1016/j.cclet.2020.12.039
1001-8417/

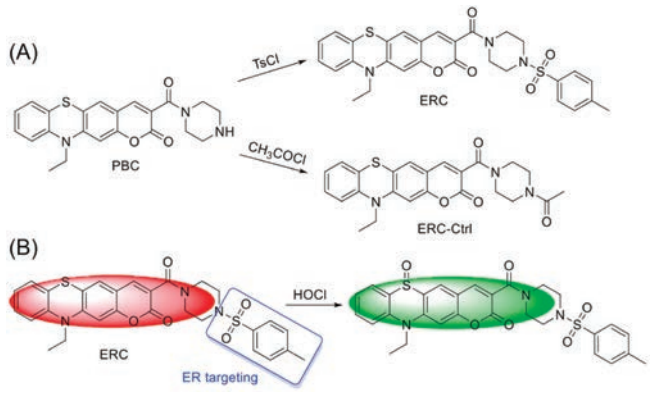

Scheme 1. (A) The preparation of ERC and ERC-Ctrl and (B) the reaction between HOCl and ERC.

selectively converted into sulfoxide by HOCl, thus leading to the blue shift in emission wavelength and facilitating the ratiometric measurement (Scheme 1). On the other hand, *p*-toluene sulfonamide (Ts) group was anchored as the ER targeting bullet [17]. Additionally, an acetamido analogue ERC-Ctrl was synthesized as a control. The probes were simply prepared from an intermediate PBC [31], and characterized by ^{1}H NMR, ^{13}C NMR, and HRMS (Supporting information).

Initially, we examined the optical behaviors of ERC toward various species, including Al^{3+}, Co^{2+}, Cu^{2+}, Hg^{2+}, Zn^{2+}, Ba^{2+}, Mg^{2+}, Mn^{2+}, Fe^{3+}, glutathione (GSH), homocysteine (Hcy), cysteine (Cys), *tert*-butyl hydroperoxide (TBHP), *tert*-butoxyl radical (TBO), $^{\bullet}OH$, $O_2^{\bullet-}$, $ONOO^-$, H_2O_2, ClO^-, and $^1O_2$. As seen in Fig. 1A, in PBS solution (pH 7.2–7.4, 10 mmol/L, containing 30% CH_3CN), the probe showed a primary absorbance at 424 nm, while a new peak was observed at 381 nm with a color change from light yellow to colorless when 30 equiv. ClO^- was added. The phenomenon was consistent with the previous reports [30,31], indicating the oxidation of the sulfur atom into sulfoxide by HOCl. When other species were added, the absorption spectra of the probe changed slightly, suggesting its specific response toward HOCl. On the other hand, the probe emitted moderate-strength fluorescence at 609 nm, while a strong emission band at 503 nm was generated upon reaction with ClO^-, accompanied by a fluorescence color change from orange red to green (Fig. 1B). A *ca.* 20-fold increment in the fluorescence ratio (F_{503}/F_{609}) was achieved accordingly (Fig. 1C). The other species induced little spectral variations and fluorescence ratio changes, reconfirming the high selectivity of ERC toward HOCl.

Subsequently, the detailed optical response of ERC toward HOCl was inspected. As depicted in Fig. 1D, upon increasing addition of ClO^-, the absorbance of the probe at 424 nm decreased gradually, and a new peak at 381 nm was strengthened. An isosbestic point at 404 nm was determined, implying the formation of a single oxidation product. The blue shift of the absorption band is ascribed to the inhibition of the intramolecular charge transfer (ICT) in the phenothiazine-derived coumarin platform after the oxidation of the sulfur atom [34,35], which was also proven by the fluorescence titration test. ERC displayed its fluorescence at 609 nm with a quantum yield (QY) of 1.03%. When ClO^- was added, a new emission band at 503 nm appeared, and the QY was elevated to 37.5% (Fig. 1E). The vibrational motions of the phenothiazine core in the probe might be the main factor accounting for its weak emission efficacy [36], while the formation of sulfoxide restricted the vibrational motions and prohibited the ICT which led to the emission enhancement with an obvious hypochromic shift. According to the titration profile, a linear relationship was found between the fluorescence ratio (F_{503}/F_{609}) of ERC and the concentrations of ClO^- in the range of 0.5–3.0 μmol/L, with a limit of detection calculated as 0.44 μmol/L (Fig. 1F).

Because of the short lifetime of HOCl in cells, a rapid detection of HOCl is required to realize real-time imaging. As illustrated in Fig. S1A (Supporting information), the fluorescence ratio of ERC showed a prominent change in seconds (< 6 s) upon addition of ClO^-, suggesting that the probe could react with intracellular HOCl

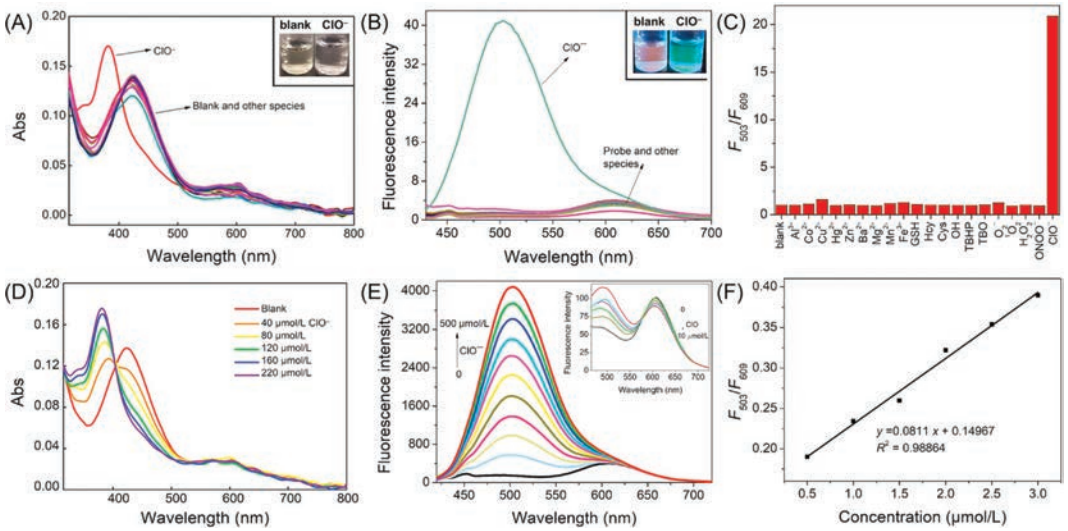

Fig. 1. (A) UV–vis absorption spectra of ERC (10 μmol/L) before and after addition of various species (1 mmol/L for GSH, Hcy, and Cys, and 300 μmol/L for the others) in PBS (pH 7.2–7.4, 10 mmol/L, containing 30% CH_3CN); Inset: the photographs of the probe solution with or without ClO^- under daylight; (B) Emission spectra of ERC (10 μmol/L) before and after addition of various species. Inset: the photographs of the probe solution with or without ClO^- under 365 nm lamp; (C) The fluorescence intensity ratio changes of ERC before and after addition of various species; (D) UV–vis absorption of ERC (10 μmol/L) in upon addition of various amount of ClO^- (0–22 equiv.); (E) Fluorescence titration of ERC (10 μmol/L) toward various amount of ClO^- (0–50 equiv.). Inset: The changes of fluorescence spectra of ERC upon addition of low concentrations of HOCl (0–10 μmol/L); (F) Linear relationship between fluorescence intensity ratios of ERC (10 μmol/L) and different concentrations of ClO^-. λ_{ex} = 390 nm; slit width: 5 nm/5 nm.

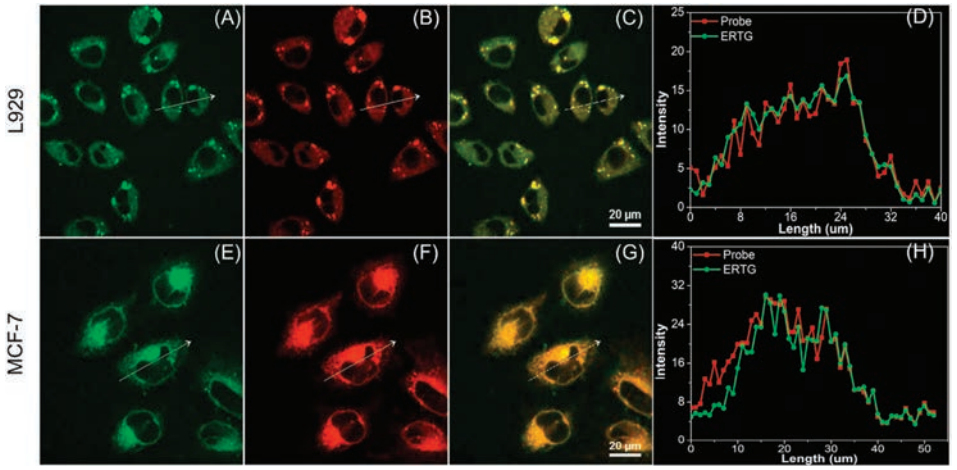

Fig. 2. Confocal fluorescence images of two cell lines stained with (A, E) 0.5 μmol/L ERTG (λ_{ex} = 488 nm, λ_{em} = 500-530 nm) and (B, F) 10 μmol/L ERC (λ_{ex} = 402 nm, λ_{em} = 552−617 nm) for 30 min. (C, G) Overlay images. (D, H) Intensity profiles of regions of interest (ROI) across cells. Scale bar: 20 μm.

rapidly to provide apparent signal response. Moreover, under continuous irradiation of Xe lamp, the fluorescence ratio of the probe with or without ClO^- kept unchanged in 25 min, showing favorable resistance against photobleaching (Fig. S1B in Supporting information). Meanwhile, the effects of pH on the optical behavior of ERC toward HOCl was also checked. In buffered solutions with different pH values ranging from 3.0 to 10, the fluorescence ratio of ERC changed negligibly. In the presence of ClO^-, evident ratio enhancement was observed in the acidic conditions with a larger one in basic solutions, signifying the efficient detecting ability of the probe in a wide pH range (Fig. S1C in Supporting information).

With the desirable properties of ERC toward HOCl in hand, we next evaluated its intracellular imaging capacity. Firstly, the cytotoxicity of ERC in normal cells (L929, mouse fibroblast cells) and cancer cells (MCF-7, human breast cancer cell line) was measured using a CCK-8 assay. After 24 h incubation with various amounts of the probe, over 80% of both types of cells kept alive when the probe concentration was less than 15 μmol/L (Fig. S2 in Supporting information), suggesting the acceptable biosecurity of the probe.

Then, the ER targetability of the probe was validated. ERC was co-cultured with commercial ER-Tracker Green (ERTG) in L929 and MCF-7 cells for 30 min before confocal imaging, respectively. As shown in Fig. 2, the red emission from ERC was distinctly visualized in both cell lines, implying its good cell membrane permeability. Furthermore, the red emission was well overlapped with the green fluorescence from ERTG with Pearson's coefficients of 0.90 in L929 cells and 0.89 in MCF-7 cells, respectively, demonstrating the dominant accumulation of ERC in the ER. To elucidate the ER-targeting ability of the Ts group, the acetamido analogue of the probe, ERC-Ctrl, was also co-cultured with ERTG in MCF-7 cells. Surprisingly, although this compound displayed similar absorbance and emission properties compared with ERC, which suggested that these two compounds had semblable brightness (Fig. S3 in Supporting information), fluorescence from ERC-Ctrl-loaded cells was much weaker than that from ERC-treated cells using the same instrumental parameters (Fig. S4 in Supporting information), indicating the frustrating cytosis of the compound. We increased the laser intensity, and constrainedly acquired its overlapped image with ERTG (Fig. S5 in Supporting information). The Pearson's coefficient was determined to be 0.53, suggesting that ERC-Ctrl showed poor targetability in the ER. Thus, the Ts group was affirmed to be pivotal not only for the ER-targetability, but also for the cellular intake.

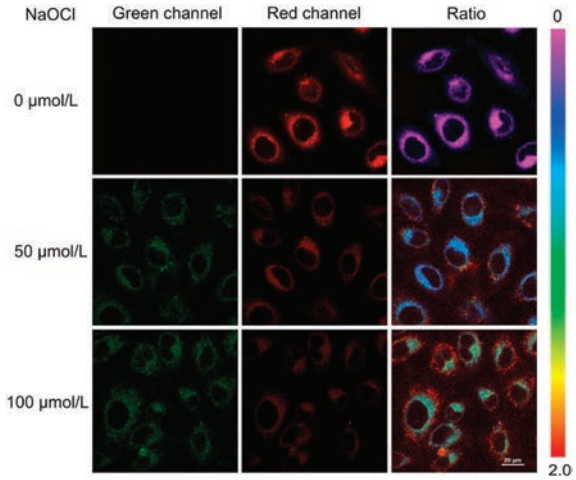

Fig. 3. Confocal fluorescence images of ERC-stained MCF-7 cells incubated with different concentrations of ClO^-. MCF-7 cells were incubated with probe (10 μmol/L) at 37 °C for 30 min, and then further treated with different amounts of ClO^- at 37 °C for 30 min. Green channel: λ_{ex} = 402 nm, λ_{em} = 500-530 nm); Red channel: λ_{ex} = 402 nm, λ_{em} = 552–617 nm). Scale bar: 20 μm.

Afterwards, the ability of ERC to detect exogenous and endogenous HOCl was examined using MCF-7 cells as model cells. As shown in Fig. 3, in ERC-stained MCF-7 cells, only red emission was observed. Upon increasing addition of ClO^-, the red fluorescence became weaker along with the elevating intensity of green light corresponding to the oxidative product. A more intuitive change can be visualized in the ratio images (F_{green}/F_{red}). In addition, MCF-7 cells were cultured with lipopolysaccharide (LPS, an inducer that can cause inflammatory responses in cells) for 30 min, and then incubated with ERC for another 30 min. Compared with the cells treated with the probe only, apparent green fluorescence appeared from LPS-stimulated cells with remarkable ratio change (Fig. 4). The combined results confirm that the probe can give sensitive ratiometric signal responses toward exogenous and endogenous HOCl in living cells.

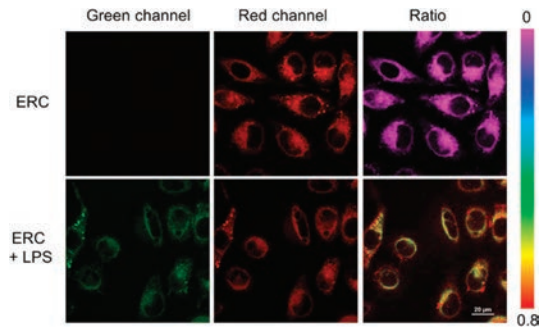

Fig. 4. Confocal fluorescence images of endogenous ClO^- in living cells. MCF-7 cells were incubated with LPS (10 μg/mL) at 37 °C for 30 min, and then further treated with ERC (10 μmol/L) for another 30 min. Green channel: λ_{ex} = 402 nm, λ_{em} = 500-530 nm; Red channel: λ_{ex} = 402 nm, λ_{em} = 552–617 nm. Scale bar: 20 μm.

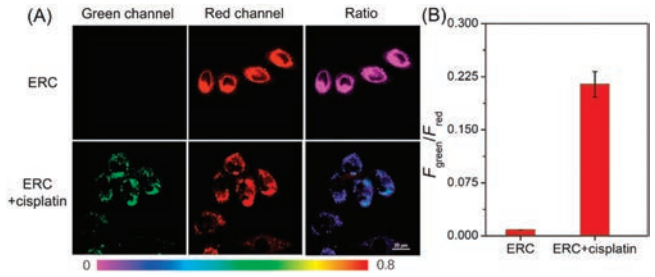

Fig. 5. Confocal fluorescence images of probe in MCF-7 cells incubated with cisplatin. MCF-7 cells were incubated with probe (10 μmol/L) at 37 °C for 30 min, and then further treated with cisplatin (100 μmol/L) at 37 °C for 15 min. Fluorescence images of MCF-7 cells from green channel (λ_{ex} = 402 nm, λ_{em} = 500-530 nm) and red channel (λ_{ex} = 402 nm, λ_{em} = 552–617 nm). Scale bar: 20 μm.

Cisplatin is one of the first-line anticancer drugs that are usually used for treatment of malignancies, such as ovarian cancer and breast cancer [37]. Mounting evidence has been presented that ER stress is involved in the cisplatin-induced cell death. In 2017, Tang *et al.* proved that $O_2^{\bullet-}$ was produced in the ER during cisplatin-stimulated cancer cells [18]. Whereas, whether the HOCl will be overexpressed in such case is still unknown. As seen in Fig. 5, in the probe-loaded MCF-7 cells, a moderate green fluorescence appeared with slight vanishment in red emission after cisplatin stimulation for 15 min. Correspondingly, a noteworthy ratio change was monitored, revealing a HOCl burst in the ER in cisplatin-treated cancer cells. Thus, our probe is potential in monitoring the HOCl up-regulation associated with anticancer drug-induced ER stress.

In conclusion, a phenothiazine-derived coumarin based fluorescent probe ERC was presented in this work. ERC can rapidly react with HOCl with sterling selectivity and sensitivity in a ratiometric manner. Ts group was proven responsible for the probe's cell membrane permeability and ER targetability. The probe was able to monitor exogenous and endogenous HOCl in the ER in living cells, and was successfully employed to detect HOCl elevation in cisplatin-treated cancer cells. This probe shows admirable properties compared with the reported ones based on sulfur oxidation (Table S1 in Supporting information) and we believe that our probe can be used to monitor HOCl variations in certain pathological processes associated with ER stress.

Declaration of competing interest

The authors report no declarations of interest.

Acknowledgment

This work was supported by the Hubei Provincial Department of Education Science and Technology Research Projects (No. Q20182704).

Appendix A. Supplementary data

Supplementary material related to this article can be found, in the online version, at doi:https://doi.org/10.1016/j.cclet.2020.12.039.

References

[1] C. Hetz, Nat. Rev. Mol. Cell Biol. 13 (2012) 89–102.
[2] D.E. Clapham, Cell 131 (2007) 1047–1058.
[3] K. Nowotny, J.P. Castro, M. Hugo, et al., Free Radical. Bio. Med. 120 (2018) 102–113.
[4] S.J. Marciniak, FEBS J. 286 (2019) 228–231.
[5] E. Bahar, J.Y. Kim, H. Yoon, Cancers 11 (2019) 338.
[6] R. Sano, J.C. Reed, BBA-Mol. Cell. Res. 1833 (2013) 3460–3470.
[7] L. Yu, J.F. Zhang, M. Li, Chem. Commun. 56 (2020) 6684–6687.
[8] N. Chaudhari, P. Talwar, A. Parimisetty, C.L. d'Hellencourt, P. Ravanan, Front. Cell. Neurosci. 8 (2014) 213.
[9] J.T. Hou, K.K. Yu, K. Sunwoo, et al., Chem 6 (2020) 832–866.
[10] D. Mennerich, S. Kellokumpu, T. Kietzmann, Antioxid. Redox Signal. 30 (2019) 113–137.
[11] Y. Zhang, H. Teng, Y. Gao, Chin. Chem. Lett. 31 (2020) 2917–2920.
[12] X. Bai, K.K.H. Ng, J.J. Hu, S. Ye, D. Yang, Annu. Rev. Biochem. 88 (2019) 605–633.
[13] X. Chen, F. Wang, J.Y. Hyun, et al., Chem. Soc. Rev. 45 (2016) 2976–3016.
[14] A.R. Lippert, G.C. Van de Bittner, C.J. Chang, Acc. Chem. Res. 44 (2011) 793–804.
[15] S. Wang, L. Chen, P. Jangili, et al., Coord. Chem. Rev. 374 (2018) 36–54.
[16] H. Xiong, L. He, Y. Zhang, et al., Chin. Chem. Lett. 30 (2019) 1075–1077.
[17] H. Xiao, P. Li, X. Hu, et al., Chem. Sci. 7 (2016) 6153–6159.
[18] H. Xiao, X. Liu, C. Wu, et al., Biosen. Bioelectron. 91 (2017) 449–455.
[19] H. Xiao, C. Wu, P. Li, B. Tang, Anal. Chem. 90 (2018) 6081–6088.
[20] M. Yan, H. Fang, X. Wang, et al., Sens. Actuators B: Chem. 328 (2021) 129003.
[21] Y. Zhao, H. Li, Z. Chai, et al., Chem. Commun. 56 (2020) 6344–6347.
[22] Y.L. Pak, S.J. Park, G. Song, et al., Anal. Chem. 90 (2018) 12937–12943.
[23] J.T. Hou, H.S. Kim, C. Duan, et al., Chem. Commun. 55 (2019) 2533–2536.
[24] Y. Lu, B. Dong, W. Song, et al., J. Photochem. Photobiol. A 384 (2019) 111980.
[25] S. Zang, X. Kong, J. Cui, et al., J. Mater. Chem. B 8 (2020) 2660–2665.
[26] T. Yang, J. Sun, W. Yao, F. Gao, Dyes Pigm. 180 (2020) 108435.
[27] Q. Xia, X. Wang, Y. Liu, et al., Spectrochim. Acta A 229 (2020) 117992.
[28] C. Duan, M. Won, P. Verwilst, et al., Anal. Chem. 91 (2019) 4172–4178.
[29] L. Huang, Y. Chen, Y. Zhao, et al., Chin. Chem. Lett. 31 (2020) 2941–2944.
[30] J.T. Hou, B. Wang, Y. Zou, et al., ACS Sens. 5 (2020) 1949–1958.
[31] J.T. Hou, B. Wang, P. Fan, et al., Dyes Pigm. 182 (2020) 108675.
[32] Y. Li, H. Li, G. Di, New J. Chem. 44 (2020) 14286–14290.
[33] J. Han, X. Liu, H. Xiong, et al., Anal. Chem. 92 (2020) 5134–5142.
[34] Y.F. Kang, L.Y. Niu, Q.Z. Yang, Chin. Chem. Lett. 30 (2019) 1791–1798.
[35] X. Yang, Y. Wang, R. Liu, et al., Sens. Actuators B 288 (2019) 217–224.
[36] L. Yao, S. Zhang, R. Wang, et al., Angew. Chem. Int. Ed. 53 (2014) 2119–2123.
[37] B. Rosenberg, Interdiscip. Sci. Rev. 3 (1978) 134–147.